LETTERS
PUBLISHED ONLINE: 29 FEBRUARY 2016 | DOI: 10.1038/NPHYS3676

nature physics

Collective magnetic response of CeO_2 nanoparticles

Michael Coey*, Karl Ackland, Munuswamy Venkatesan and Siddhartha Sen

The magnetism of nanoparticles and thin films of wide-bandgap oxides that include no magnetic cations is an unsolved puzzle[1]. Progress has been hampered by both the irreproducibility of much of the experimental data, and the lack of any generally accepted theoretical explanation. The characteristic signature is a virtually anhysteretic, temperature-independent magnetization curve that saturates in an applied field that is several orders of magnitude greater than the magnetization. It would seem as if a tiny volume fraction, $\lesssim$0.1%, of the samples is magnetic and that the energy scale is unusually high for spin magnetism. Here we investigate the effect of dispersing 4 nm CeO_2 nanoparticles with powders of γAl_2O_3, sugar or latex microspheres. The saturation magnetization, $M_s \approx 60$ A m^{-1} for compact samples, is maximized by 1 wt% lanthanum doping. Dispersing the CeO_2 nanopowder reduces its magnetic moment by up to an order of magnitude, and there is a characteristic length scale of order 100 nm for the magnetism to appear in CeO_2 nanoparticle clusters. The phenomenon is explained in terms of a giant orbital paramagnetism that appears in coherent mesoscopic domains due to resonant interaction with zero-point fluctuations of the vacuum electromagnetic field. The theory explains the observed temperature-independent magnetization curve and its doping and dispersion dependence, based on a length scale of 300 nm that corresponds to the wavelength of a maximum in the ultraviolet absorption spectrum of the magnetic CeO_2 nanoparticles. The coherent domains occupy roughly 10% of the sample volume.

There is a class of thin films and nanoparticles of oxides that exhibit ferromagnetic-like magnetization curves, although the materials lack the concentration of ions with unpaired d or f electron spins required to generate the exchange interactions needed for high-temperature ferromagnetism[1]. This is forcing a re-evaluation of the meaning of magnetic saturation in systems that exhibit very little hysteresis. Research in this area has been plagued by a shortage of reproducible experimental data, so there is need for an easily synthesized 'fruitfly' system that reliably exhibits stable anomalous magnetism for which no extraneous explanation is possible. The much-studied dilute Co-doped ZnO thin films[2] were problematic because metallic cobalt nanoparticles, difficult to detect in ZnO films[1–4], are ferromagnetic with a high Curie temperature.

The reports of magnetism in these oxide systems have shown that a 3d dopant is unnecessary, and even when 3d ions are present they do not necessarily order magnetically[5–8]. The magnetism is somehow related to defects; candidates include cation[9] or oxygen[10] vacancies (F-centres). Sundaresan *et al.*[11] have suggested that weak room-temperature magnetism could actually be a general feature of oxide nanoparticles. A significant observation was that the magnetism appearing in undoped 10 nm ZnO nanoparticles depends on how they are capped with different molecules, which alter the electronic structure of the surface[12].

A promising candidate system is CeO_2, where nanoparticles produced in different laboratories often exhibit weak 'ferromagnetic-like' behaviour at room temperature. A selection of data is presented in Table 1. Although values of saturation magnetization M_s are very small and vary widely, the saturation field H_0 obtained by extrapolating the initial susceptibility to saturation is roughly 1,000 times greater and lies in a narrower range of 40–120 kA m^{-1}. The ratio $N_{\rm eff}M_s/H_0$ with an effective demagnetizing factor $N_{\rm eff} \approx 0.3$ is a measure of the magnetic volume fraction f in a ferromagnetic system where the approach to saturation is governed by dipolar interactions[1]. In that case f would be of the order of 0.1%.

We synthesized many small batches ($\sim$4 mg) of nanocrystalline CeO_2 powder using as precursor either high-purity (99.999%) $Ce(NO_3)_3{\cdot}6H_2O$, or reagent-grade (99%) with La as the main impurity. The nanoparticles are well crystallized, and only $2r = 4$ nm in diameter (Fig. 1a,b). Magnetization curves of nanoparticles produced from the two precursors are compared in Fig. 2a. The pure sample shows a practically linear paramagnetic response, but the impure sample exhibits a superposed ferromagnetic-like curve with no evidence of hysteresis. The averaged specific magnetization σ_s for 16 samples is 0.011 ± 0.006 A m^2 kg^{-1}, corresponding to an average moment per Ce ion of $3 \times 10^{-4}\,\mu_B$ and an average saturation magnetization $M_s = 84$ A m^{-1}. These numbers can be misleading. There is evidence that the moment is associated with defects[13–15] or with the nanoparticle surface[12,16] rather than cerium ions distributed homogeneously throughout the volume, so it is better to think of a few tenths of a Bohr magneton as the average moment per particle. The content of Fe, Co and Ni impurities in the 99% CeO_2 nanoparticles—10 ppm in total—is too little to account for the observed moments, because each nanoparticle contains approximately 900 cerium atoms.

In fact, it is the lanthanum doping that is responsible for the moment. On doping the pure cerium nitrate precursor with pure lanthanum nitrate, there is a sharp maximum in magnetization for $Ce_{1-x}La_xO_2$ at $x = 1.0$% and the moment has almost disappeared at $x = 10$% (Fig. 2b). A similar decline has been observed for Pr doping[14]. The moments are fairly stable in time, decaying by about a tenth over the course of two years. Moreover, the magnetization curves between 4 K and 380 K superpose after correcting for the high-field slope (Fig. 2c), with little sign of hysteresis at any temperature. The insensitivity of the magnetization to thermal excitations, at least up to 380 K, is evidence that an unusually large energy scale >0.1 eV must be involved.

Like Ce^{4+}, La^{3+} has a $4f^0$ configuration, so La substitution in stoichiometric CeO_2 would normally create holes at the top of the oxygen 2p band. However, CeO_2 is a catalyst renowned for its oxygen

School of Physics and CRANN, Trinity College, Dublin 2, Ireland. *e-mail: jcoey@tcd.ie

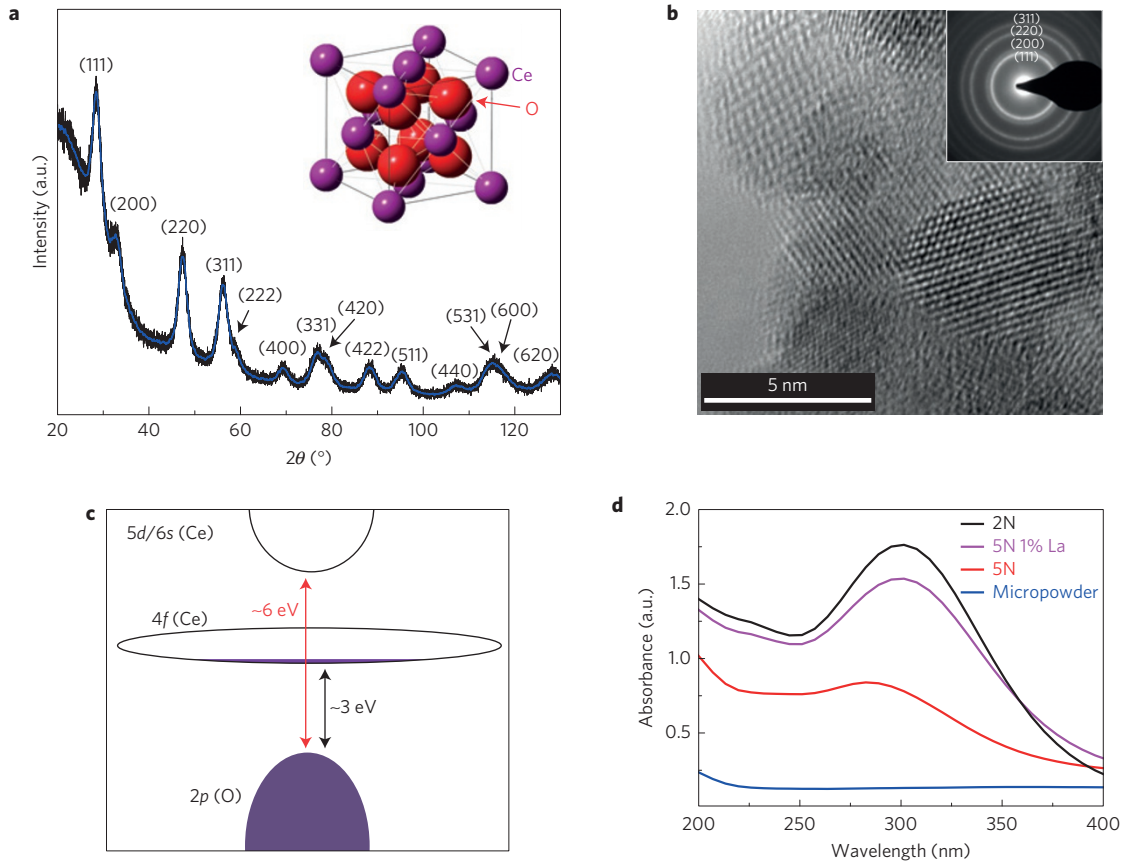

Figure 1 | Structure and optical properties of 4 nm CeO_2 nanoparticles. a, X-ray diffraction pattern showing the reflections of the fluorite structure, with corresponding particle size broadening. **b**, Transmission electron micrograph of a few of the particles. **c**, Schematic electronic structure of oxygen-deficient CeO_2. **d**, Ultraviolet–visible absorption spectra of CeO_2 micropowders and nanopowders dispersed in 0.1 M H_2SO_4. The spectra of the magnetic nanoparticles show a peak at 4 eV.

vacancies, and the addition of La increases the quantities of both oxygen vacancies and peroxide ions that occur naturally at the CeO_2 surface[17]. The content of localized Ce^{3+} ions estimated from the Curie-law variation of the susceptibility (Fig. 2d) is only 0.4%. If there are any other Ce^{3+} electrons, they are delocalized at the bottom of the 4*f* band as suggested in Fig. 1c. The 2*p*–4*f* gap for stoichiometric CeO_2 is 3.0–3.5 eV and the 2*p*–5*d*/6*s* gap is 6–8 eV (refs 18,19). Electrons will tend to segregate to the nanoparticle surface, which is conducting for oxygen-deficient CeO_2 (refs 19,20). It should be emphasized that Ce^{3+} compounds or intermetallics rarely order magnetically above 15 K (1.3 meV), and the maximum reported value is 125 K (ref. 21).

In a series of experiments where the CeO_2 nanopowder was progressively diluted with powders of different particle size, we used a 15 nm γAl_2O_3 nanopowder, finely ground icing sugar with an average particle size ~1 μm and latex microspheres 10 μm in diameter. The surprising effect of dispersion with γAl_2O_3 is shown in Fig. 3a. When a 4 mg sample of CeO_2 is diluted with six times its own volume of diamagnetic γAl_2O_3, the magnetic moment collapses to just 6% of the original value (Fig. 3). The effect of dilution is to separate clumps of CeO_2 nanoparticles $\leq$ 100 nm in size. Dilution with finely ground sugar has a similar, if less pronounced effect. The moment there falls by 50% on diluting with 30 times the volume of sugar, which is less effective than γAl_2O_3 at dispersing the CeO_2 particles, but has the advantage that some of the CeO_2 can be recovered by dissolving the sugar in water. The specific magnetization for the recovered CeO_2 is double that at the outset. Large, 10 μm latex microspheres are least effective; the moment is reduced by 15% for a 20-fold volume dilution. The aggregates of CeO_2 coexisting with the microspheres are about 500 nm in size, and sometimes envelop them (Fig. 3d).

Together, these experiments establish that the magnetism of CeO_2 depends critically on the mesoscale disposition of the

Table 1 | A selection of magnetization data reported for CeO_2 nanoparticles, together with the extrapolated saturation field H_0 and the magnetic volume fraction *f*.

Average radius r_0 (nm)	M_s (A m^{-1})	H_0 (kA m^{-1})	f^* (10^{-6})	Surface treatment	Reference
3.5	7	60	39	—	ref. 16
7.5	11	40	92	—	ref. 16
5 × 1 needles	550	80	2,290	PEG	ref. 29
3	40	80	168	Oleic acid	ref. 30
3.5	1.5	120	4	Glutamic acid	ref. 31
2.7	25	70	120	NH_4OH	ref. 32
1.8	760	50	5,060	1,2 dodecanediol	ref. 33
2.5	150	32	1,560	PEG	ref. 23
4.6	120	110	364	PVP	ref. 34
3.0	140	90	520	—	ref. 14
2.0	84(46)	120(38)	233	PEG	This work†

*Calculated using N_{eff} = 1/3. †Standard deviations for 16 samples.

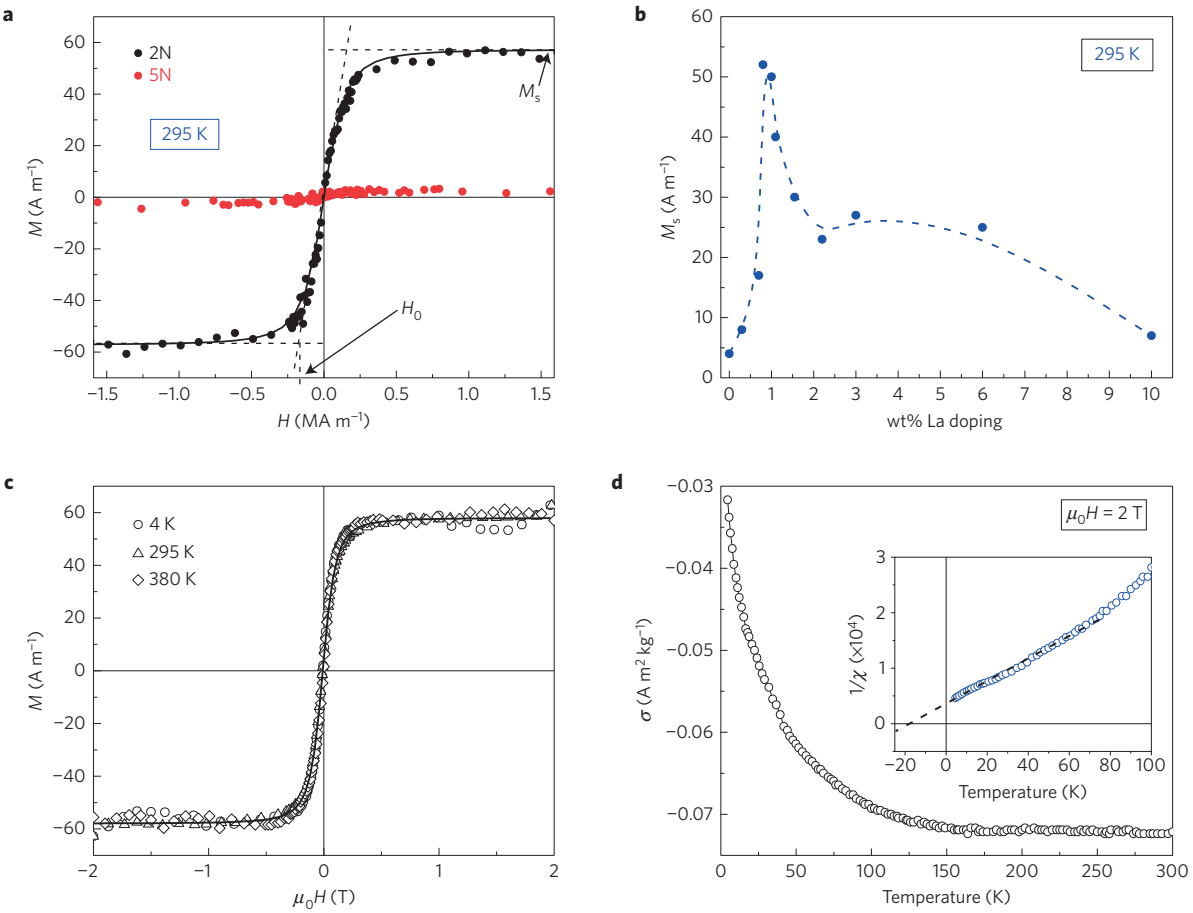

Figure 2 | Magnetic properties of 4 mg samples of 4 nm CeO_2 nanoparticles. a, Room-temperature magnetization curves of samples prepared from 99.999% and 99% precursors; the saturation magnetization M_s and the saturation field H_0 are defined as shown. **b**, The variation of M_s for nanoparticles produced from the pure precursor with La nitrate addition; magnetization is turned on by La substitution, and it is greatest for a La content of 1%. **c**, Magnetization curves of a 99% sample at 4 K, 295 K and 380 K. The data are corrected for the diamagnetism of the sample holder and the high-field susceptibility of the sample; the magnetization curves are fitted to equation (2), yielding identical parameters at all temperatures. **d**, The Curie law susceptibility deduced from the high-field slope. The plot of susceptibility versus inverse temperature in the inset corresponds to just 0.4% of Ce^{3+} and a paramagnetic Curie temperature of −8 K, assuming a localized moment of $p_{eff} = 2.54\mu_B$.

nanoparticles, as well as doping, which is probably why there is so much variability in the data of Table 1. We conclude that there is a characteristic length scale for the appearance of magnetism, which is of order 100 nm. Previously, it had been reported that the moment of 6 nm nanoparticles of ZnO doped with 0.93% Ni appeared only in reaction-limited aggregates about 400 nm in size[22], and that the moment in 7 nm CeO_2 powder was modified on sintering[13]. The magnetism is not simply an intrinsic property governed by atomic-scale defects within the particles. The extent and topology of the surface of contiguous particles is a critical factor.

Until now, a plausible model for the high-temperature magnetism of CeO_2 nanoparticles has been Stoner ferromagnetism with a spin-split band associated with conducting surface states[23]. Furthermore, if the band is half-metallic, spin-wave excitations are suppressed, and a high Curie temperature could be envisaged[24]. The problem is to understand how, when we break up the CeO_2 nanoparticle sample into 100 nm clumps, we can lose the magnetism. Stoner splitting of a 4f band or a defect band, of order a few tenths of an electron volt, will not change appreciably when the sample is divided up. The closest analogy in the conventional paradigm is the stabilization of magnetic order in clusters of superparamagnetic nanoparticles by dipole–dipole interactions[25]. The magnetite particle chains in magnetotactic bacteria are a good example. Contiguous particles with a magnetization of order 0.5 MA m^{-1} and a moment of order 1,000μ_B can provide a dipole interaction energy that exceeds room temperature. However, the average moment of a CeO_2 nanoparticle is three or four orders of magnitude too small for this explanation to work.

It seems that a radically new approach is required. We propose that the magnetic saturation is not related to collective spin ferromagnetism but to giant orbital paramagnetism[26] associated with the collective response of electrons in coherent domains to an applied magnetic field. Our starting point is a new model[27], which showed that when zero-point fluctuations of the vacuum electromagnetic field interact with an ensemble of two-level atoms, it is possible for coherent mesoscopic domains to emerge. This can take place at room temperature in quasi-two-dimensional systems, with a large surface/volume ratio. No resonant cavity is required. The size of the coherent domains is determined by the wavelength corresponding to an electronic excitation $\hbar\omega$ between the ground state and the excited state of the two-level atoms. The excited state lies at an energy ε below the ionization threshold, as illustrated in Fig. 4a. The interaction of the N electrons in a coherent domain of size $\lambda \approx 2\pi c/\omega$ with the vacuum field leads to stabilization of the ground state and destabilization of the excited state each by an energy $G^2\hbar\omega$, where G is calculated to be ≈0.1 (ref. 27). The model is parameterized in terms of N, ω and ε, and the stability condition is $k_B T < G^2\hbar\omega < \varepsilon$.

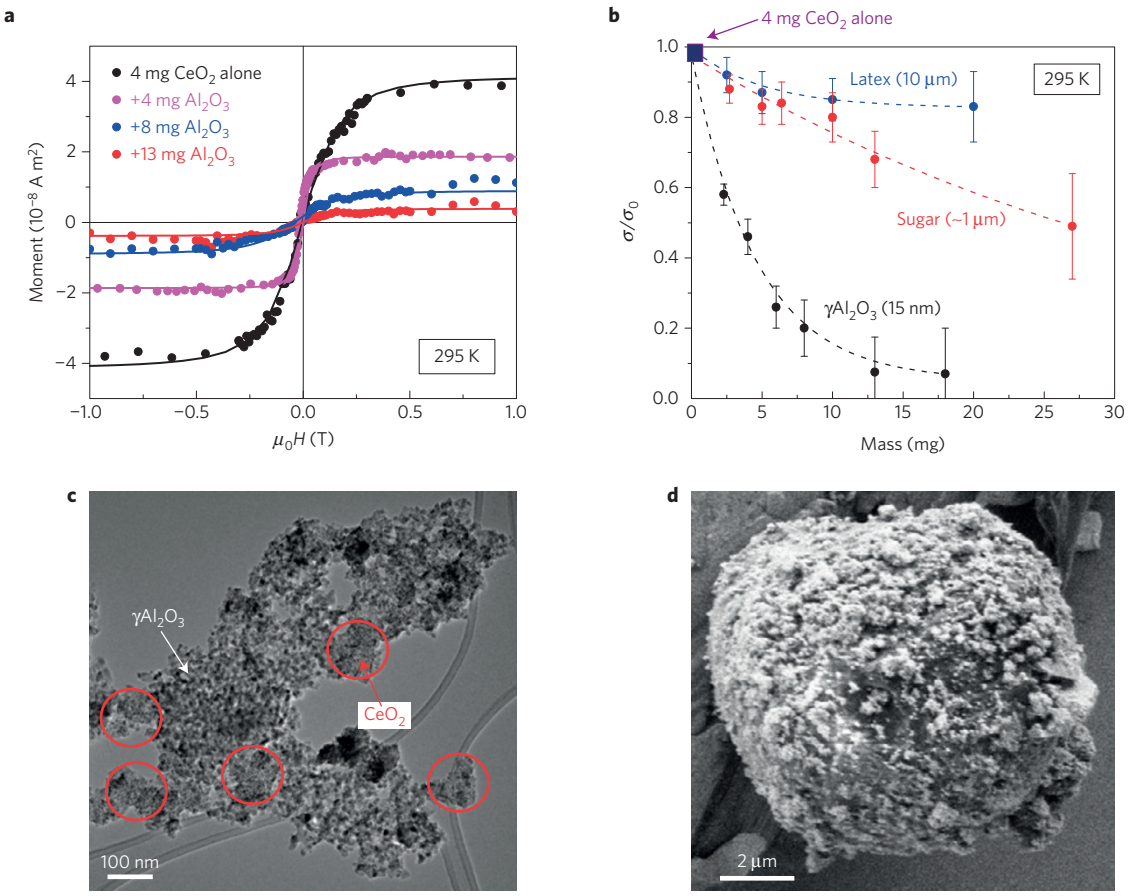

Figure 3 | Effect on magnetic moment of diluting the CeO_2 with another powder. a, Magnetization curves for a 4 mg sample of 4 nm CeO_2 nanopowder diluted with 15 nm γAl_2O_3. **b**, Relative magnetization as a function of dilution of 4 mg of 4 nm CeO_2 by weight with 15 nm γAl_2O_3, 1 μm sugar or 10 μm latex microspheres. Error bars represent standard deviations of measurements on multiple batches. **c**, Electron micrograph, showing how the dilution with γAl_2O_3 breaks the CeO_2 down into ~100 nm clumps, which destroys the moment. **d**, The coating of a 10 μm latex microsphere by CeO_2 nanoparticles.

In the coherent ground state, the electrons have a common induced oscillation frequency $G^2\omega$ and a corresponding moment (see Supplementary Information)

$$\mu_c = [(2l+3)(2l+4)/8](G^2\hbar\omega/2\varepsilon)\mu_B \quad (1)$$

that is set by the size of the orbit, where l is the orbital quantum number of the electronic ground state and μ_B is the Bohr magneton. In the presence of the time-varying vacuum electromagnetic field, the effect of a static magnetic field on the coherent domain is to produce a modified coherent ground state, inducing a paramagnetic orbital moment in the domain that is nonlinear in B and proportional to $\sin 2\alpha_m$, where α_m is a mixing angle (see Supplementary Information). The magnetization curve has the form

$$M = M_s x/(1+x^2)^{1/2} \quad (2)$$

where $x = CB \approx GN\mu_c B/\hbar\omega$. This function differs only slightly from the empirical $M = M_s \tanh y$ function often used to fit magnetization curves[23], but it follows directly from theory. Fits of equation (2) to the curves in Fig. 2c at 4 K, 295 K and 380 K give very similar fit parameters $C = 9.4 \pm 0.7\ T^{-1}$ and $M_s = 58 \pm 1\ A\ m^{-1}$.

The length scale in the problem is set by a characteristic excitation frequency ω of CeO_2, which is resonant with the zero-point vacuum fluctuations. The corresponding wavelength is $\lambda = 2\pi c/\omega$, and the volume of the coherent domain is $v_c \approx (\pi/6)\lambda^3$. In Fig. 1d there is a prominent absorption at $\lambda = 300$ nm in the ultraviolet spectrum of the magnetic nanoparticles. The corresponding frequency of the electronic transition is $\omega = 6.3 \times 10^{15}\ s^{-1}$, and the photon energy is $\hbar\omega = 4.1$ eV. No real photons of this energy are emitted or absorbed according to the theory[27]; it is the zero-point energy that owing to its time dependence can mix states that differ in energy by $\hbar\omega$ to produce a modulated collective response frequency for all N electrons in a coherent domain.

By fitting the magnetization curve to equation (2), we can deduce the volume fraction f_c of the sample that is composed of coherent domains, and estimate their magnetic moment $N\mu_c$. Dividing the saturation magnetization $M_s \approx f_c GN\mu_c/2v_c$, by $C \approx GN\mu_c/\hbar\omega$, we obtain $M_s/C = f_c\hbar\omega/2v_c$. With the experimental value of M_s/C and $G \approx 0.1$, we find $f_c = 28\%$ and the coherent domain moment $N\mu_c = 6.6 \times 10^6 \mu_B$. Identifying N with the number of La dopant atoms in a coherent domain (2.4×10^6), the coherent moment per dopant $\mu_c = 2.8\mu_B$.

The orbital moment expected from equation (1) depends on G, the orbital quantum number of the ground state and the ionization energy ε of the excited state. Taking $G \approx 0.1$ and $l = 3$, identifying the transition that becomes very prominent in the magnetic nanoparticles (Fig. 1d) as a $4f$–$5d$ transition, the ionization energy $\varepsilon \approx 0.1$ eV. The values of G and N are in accord with the values anticipated for quasi-two-dimensional coherent domains in the model[27] ($G \approx 0.1$ and $N \approx 10^6$ for $\hbar\omega = 4.1$ eV). The model of ref. 27 was simplified, and took no account of the spin of the electrons. The influence of spin–orbit coupling and taking account of Fermi–Dirac statistics in these dilute electronic systems will not modify the semiquantitative agreement between the theory and our experiments. Generally, it will be possible to estimate the size λ of the

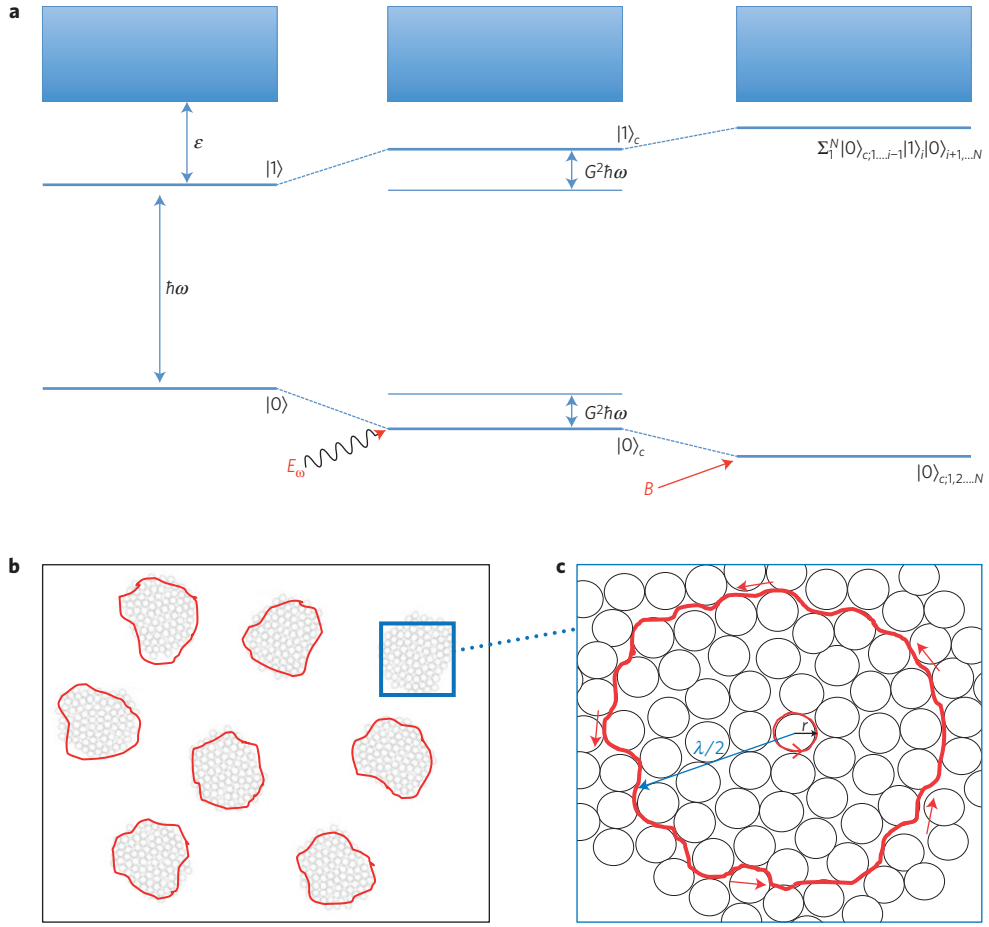

Figure 4 | Coherent mesoscopic domains in CeO_2. a, Single-atom electronic excitations related to impurities or defects in CeO_2, showing the effect of coherent interaction with the vacuum electromagnetic field and the consequent influence of a magnetic field on the ground and excited states. **b**, A sample of CeO_2 where a fraction f of the volume is occupied by coherent domains of dimension $\lambda = 2\pi c/\omega$ (shaded grey). **c**, An orbital current in a coherent domain formed from a clump of CeO_2 nanoparticles.

coherent domains in such systems by fitting the magnetization curve to equation (2) to determine C/M_s and then using the following expression that follows from $\hbar\omega = 2\pi\hbar c/\lambda$, $M_s/C = f_c\hbar\omega/2v_c$ and $v_c = \pi\lambda^3/6$

$$\lambda = [(C/M_s)(6\hbar c\, f_c)]^{1/4} \sim [(C/M_s)\hbar c]^{1/4} \qquad (3)$$

In summary, giant orbital moments related to zero-point fluctuations of the vacuum electromagnetic field can resolve a long-standing problem in magnetism. The theory accounts for the temperature independence of the magnetization curve, and the characteristic length scale of order 100 nm required for the appearance of the magnetically induced orbital currents in coherent domains. The saturation magnetization M_s and the parameter C in equation (2), which are easily obtained by fitting the magnetization curve, determine the size of the coherent domains through equation (3) and the value of their giant orbital moments, assuming $G \approx 0.1$. The data on all our magnetic samples, and almost all the other data in Table 1, are consistent with $\lambda \approx 300$ nm, and coherent volume fractions of 1–80%.

Giant orbital paramagnetism is a new observable consequence of zero-point electromagnetic energy—it is the first such magnetic effect. It occurs in mesoscopic quasi-two-dimensional matter where the active sites are dilute and the effects of Fermi–Dirac statistics can be neglected. Spin–orbit interaction is expected to stabilize the coherent state. It is anticipated that the present study will lead further investigations of measurable consequences of resonant zero-point fluctuations not only in magnetic systems such as gold nanoparticles[28], but in other areas of condensed matter, whether physics, chemistry or biology. Some candidate systems are nanobubbles, the water/cell interface and concentrated ionic solutions.

Methods

Methods and any associated references are available in the online version of the paper.

Received 30 November 2015; accepted 22 January 2016; published online 29 February 2016

References

1. Coey, J. M. D. *Handbook of Spin Transport and Magnetism* Ch. 20, 405–426 (CRC Press, 2012).
2. Pan, F., Song, C., Liu, X. J., Yang, Y. C. & Zeng, F. Ferromagnetism and possible application in spintronics of transition-metal doped ZnO films. *Mater. Sci. Eng. R* **62,** 1–35 (2008).
3. Park, J. H. *et al*. Co metal clustering as the origin of ferromagnetism in Co-doped ZnO thin films. *Appl. Phys. Lett.* **84,** 1338–1340 (2004).
4. Dorneles, L. S. *et al*. Magnetic and structural properties of Co-doped ZnO thin films. *J. Magn. Magn. Mater.* **310,** 2087–2088 (2007).
5. Barla, A. *et al*. Paramagnetism of the Co sublattice in ferromagnetic $Zn_{1-x}Co_xO$ films. *Phys. Rev. B* **76,** 125201 (2007).
6. Tietze, T. *et al*. XMCD studies on Co and Li doped ZnO magnetic semiconductors. *New J. Phys.* **10,** 055009 (2008).
7. Venkatesan, M. *et al*. Room-temperature ferromagnetism in Mn- and Fe-doped indium tin oxide thin films. *J. Appl. Phys.* **103,** 07D135 (2008).

8. Coey, J. M. D., Gunning, R. D., Venkatesan, M., Stamenov, P. & Paul, K. Magnetism in defect-ridden oxides. *New J. Phys.* **12,** 053025 (2010).
9. Elfimov, I. S., Yunoki, S. & Sawatzky, G. A. Possible path to a new class of ferromagnetic and half-metallic ferromagnetic materials. *Phys. Rev. Lett.* **89,** 216403 (2002).
10. Banerjee, S., Mandal, M., Gayathri, N. & Sardar, M. Enhancement of ferromagnetism upon thermal annealing in pure ZnO. *Appl. Phys. Lett.* **91,** 182501 (2007).
11. Sundaresan, A. *et al*. Ferromagnetism as a universal feature of nanoparticles of otherwise nonmagnetic oxides. *Phys. Rev. B* **74,** 161306(R) (2006).
12. Chaboy, J. *et al*. Evidence of intrinsic magnetism in capped ZnO nanoparticles. *Phys. Rev. B* **82,** 064411 (2010).
13. Fernandez, V. *et al*. Ferromagnetism induced by oxygen and cerium vacancies above the percolation limit in CeO_2. *J. Phys. Condens. Matter* **22,** 216004 (2010).
14. Paunovic, N. *et al*. Suppression of inherent ferromagnetism in Pr-doped CeO_2 nanocrystals. *Nanoscale* **4,** 5469–5476 (2012).
15. Chen, S. Y. *et al*. Concentration dependence of oxygen vacancy on the magnetism of CeO_2 nanoparticles. *J. Phys. Chem. C* **116,** 8707–8713 (2012).
16. Sundaresan, A. & Rao, C. N. R. Ferromagnetism as a universal feature of inorganic nanoparticles. *Nano Today* **4,** 96–106 (2009).
17. Keating, P. R. L., Scanlon, D. O. & Watson, G. W. The nature of oxygen states on the surfaces of CeO_2 & La-doped CeO_2. *Chem. Phys. Lett.* **608,** 239–243 (2014).
18. Xiao, X., Jerratsch, J. F., Nilius, N. & Freund, H. J. Probing the 4*f* states of ceria by tunelling spectroscopy. *Phys. Chem. Chem. Phys.* **13,** 12646–12651 (2011).
19. Gillen, R., Clark, S. J. & Robertson, J. Nature of the electronic band gap in lanthanide oxides. *Phys. Rev. B* **87,** 125116 (2013).
20. Popovic, Z. V., Dohcevic-Mitrovic, Z. D., Paunovic, N. & Radovic, M. Evidence of charge delocalization in $Ce_{1-x}Fe_x^{2+(3+)}O_{2-y}$ nanocrystals ($x = 0$, 0.06, 0.12). *Phys. Rev B* **85,** 014302 (2012).
21. Givord, F. *et al*. Ferromagnetism and crystal electric field in the cerium compound $CeRh_3B_2$. *J. Phys. Condens. Matter* **19,** 356208 (2007).
22. Radovanovic, P. V. & Gamelin, D. R. High-temperature ferromagnetism in Ni^{2+}-doped ZnO aggregates prepared from colloidal dilute magnetic semiconductor quantum dots. *Phys Rev. Lett.* **91,** 157302 (2003).
23. Ackland, K., Monzon, L. M. A., Venkatesan, M. & Coey, J. M. D. Magnetism of nanostructured CeO_2. *IEEE Trans. Magn.* **47,** 3509–3512 (2011).
24. Edwards, D. M. & Katsnelson, M. I. High-temperature ferromagnetism of *sp* electrons in narrow impurity bands: application to CaB_6. *J. Phys. C* **18,** 7209–7225 (2006).
25. Bedanta, S. & Kleemann, W. Supermagnetism. *J. Phys. D* **42,** 013001 (2009).
26. Hernando, A., Crespo, P. & Garcia, M. A. Origin of orbital ferromagnetism and giant magnetic anisotropy at the nanoscale. *Phys. Rev. Lett.* **96,** 057206 (2004).
27. Sen, S., Gupta, K. L. & Coey, J. M. D. Mesoscopic structure formation in condensed matter due to vacuum fluctuations. *Phys. Rev. B* **92,** 155115 (2015).
28. Nealon, G. L. *et al*. Magnetism in gold nanoparticles. *Nanoscale* **4,** 5244–5258 (2012).
29. Liu, Y. *et al*. Size dependent ferromagnetism in cerium oxide (CeO_2) nanostructures independent of oxygen vacancies. *J. Phys. Condens. Matter* **20,** 165201 (2008).
30. Ge, M. Y. *et al*. On the origin of ferromagnetism in CeO_2 nanocubes. *Appl. Phys. Lett.* **93,** 062505 (2008).
31. Chen, X. *et al*. Synthesis and room-temperature ferromagnetism of CeO_2 nanocrystals with nonmagnetic Ca^{2+} doping. *Nanotechnology* **20,** 115606 (2009).
32. Li, M. *et al*. Relationship between the surface chemical states and magnetic properties of CeO_2 nanoparticles. *Appl. Phys. Lett.* **94,** 152511 (2009).
33. Chen, S. Y. *et al*. Oxygen vacancy dependent magnetism of CeO_2 nanoparticles prepared by thermal decomposition method. *J. Phys. Chem. C* **114,** 19576–19581 (2010).
34. Phokha, S. *et al*. Synthesis, characterization, and magnetic properties of monodisperse CeO_2 nanospheres prepared by PVP-assisted hydrothermal method. *Nanoscale Res. Lett.* **7,** 425 (2012).

Acknowledgements

This work was supported by Science Foundation Ireland as part of the NISE project, contract 10/IN1.I3006.

Author contributions

M.C. conceived the experiment and wrote the paper, K.A. and M.V. carried out the experiments and reduced the data, S.S. developed the theory, and M.C. and S.S. analysed the results.

Additional information

Supplementary information is available in the online version of the paper. Reprints and permissions information is available online at www.nature.com/reprints. Correspondence and requests for materials should be addressed to M.C.

Competing financial interests

The authors declare no competing financial interests.

Methods

The CeO_2 nanoparticles were synthesized by homogeneous precipitation[23] from 10 mM $Ce(NO_3)_3{\cdot}6H_2O$ solutions by dropwise addition of 0.1 M NaOH (99.99% purity). Then 0.45 ml (1/10 the volume of $Ce(NO_3)_3{\cdot}6H_2O$ solution) of 0.5 M polyethylene glycol (PEG) with molecular weight 1,500 is added to help separate the nanoparticles during formation; they are well crystallized, but only about 4 nm in size (Fig. 1). Magnetization was measured on 4 mg samples of CeO_2 nanoparticles using a 5 T Quantum Design SQUID magnetometer. Powders were contained in gelcap sample holders, which produce a linear diamagnetic response, mounted in a plastic straw. All isothermal magnetization curves, but not the thermal scans, have been corrected for the linear response.